Journal of Inorganic Biochemistry 223 (2021) 111537

Contents lists available at ScienceDirect

Journal of Inorganic Biochemistry

journal homepage: www.elsevier.com/locate/jinorgbio

Phosphorescent rhenium(I) complexes conjugated with artesunate: Mitochondrial targeting and apoptosis-ferroptosis dual induction

Rui-Rong Ye [*,1], Bi-Chun Chen [1], Jun-Jian Lu, Xiu-Rong Ma, Rong-Tao Li [*]

Faculty of Life Science and Technology, Kunming University of Science and Technology, Kunming 650500, PR China

ARTICLE INFO

Keywords:
Rhenium(I) complex
Artesunate
Mitochondria
Anticancer activity
Apoptosis
Ferroptosis

ABSTRACT

Cell death is essential for cancer, which can be induced through multiple mechanisms. Ferroptosis, a newly emerging form of non-apoptotic cell death, involves the generation of iron-dependent reactive oxygen species (ROS). In this study, we designed and synthesized two artesunate (ART) conjugated phosphorescent rhenium(I) complexes (Re(I)-ART conjugates), $[Re(N^{\wedge}N)(CO)_3(PyCH_2OART)](PF_6)$ (**Re-ART-1** and **Re-ART-2**) (Py = pyridine, N^N = 1,10-phenanthroline (phen, in **Re-ART-1**) and 4,7-diphenyl-1,10-phenanthroline (DIP, in **Re-ART-2**)) that can specifically locate in the mitochondria of human cervical carcinoma (HeLa). Mechanism studies show that **Re-ART-1** and **Re-ART-2** exhibit high cytotoxicity against cancer cells lines and can induce both apoptosis and ferroptosis in HeLa cells through mitochondrial damage, caspase cascade, glutathione (GSH) depletion, glutathione peroxidase 4 (GPX4) inactivation and lipid peroxidation accumulation. As a result, this work presents the rational design of Re(I)-ART conjugates as a promising strategy to induce both apoptosis and ferroptosis and improve therapeutic efficiency of cancer treatment.

1. Introduction

Rhenium(I) organometallic complexes with rich photophysical and photochemical properties have been developed as luminescent probes [1,2]. $^{186/188}$Re is widely used as radio-pharmaceuticals [3]. Recently, rhenium(I) tricarbonyl complexes, one class of the rhenium(I) organometallic complexes, have been extensively reported as anticancer agents [4–7]. For instance, Mao and Tan et al. [8] reported that rhenium(I) tricarbonyl complexes could accumulate in mitochondria and subsequently cause cell death by exerting irreversible oxidative stress and glutathione (GSH) metabolism disorder. Wilson et al. reported a rhenium isonitrile complex that can induce apoptosis mediated by unfolded protein response, which also exhibits in vivo and in vitro anticancer activity and resistance to ovarian cancer cells [9–11]. The rhenium complexes designed by Massi et al. can induce cell cycle arrest by inhibiting the phosphorylation of Aurora-A kinase [12]. Falasca et al. reported that rhenium complexes can block the spread of cancer by inhibiting the signal cascade induced by fibroblast growth factor receptor [13], and sarcoma. Zobi et al. synthesized a Re(I) tricarbonyl complex with selective cytotoxicity towards HCT-116 cells [14]. We previously designed and synthesized a rhenium(I)-based histone deacetylase inhibitor, which could target mitochondria and suppress histone deacetylases activity [15]. We also explored the anticancer mechanisms of mononuclear and dinuclear rhenium(I) complexes, which were closely associated with organelle-specific localization [16]. In summary, the possibility of oncotherapy and superior luminescent properties of rhenium(I) tricarbonyl complexes make them meaningful for future anti-cancer drug research.

Abbreviations: ART, Artesunate; ROS, Reactive oxygen species; GSH, Glutathione; GSSH, Oxidized glutathione; RCD, Regulated cell death; GPX4, Glutathione peroxidase IV; MDA, Malondialdehyde; DMEM, Dulbecco's Modified Eagle Medium; FBS, Fetal bovine serum; PBS, Phosphate-buffered saline; DCC, Dicyclohexylcarbodiimide; DMAP, 4-*N*,*N*-dimethylaminopyridine; PLE, Porcine liver esterase; HPLC, High performance liquid chromatography; ICP-MS, Inductively coupled plasma mass spectrometry; MTT, 3-(4,5-dimethylthiazol-2-yl)-2,5-diphenyltetrazolium bromide; MTDR, MitoTracker Deep Red FM; LTDR, LysoTracker Deep Red FM; CCCP, Cyanide 3-chlorophenylhydrazone; MMP, Mitochondrial membrane potential; Rh123, Rhodamine 123; H_2DCFDA, 2′,7′-dichlorodihydrouorescein diacetate; DCF, 2′,7′-dichlorodihydrouorescein; Hoechst 33342, 2′-(4-ethoxyphenyl)-5-(4-methyl-1-piperazinyl)-2,5′-bi-1H-benzimidazole trihydrochloride; ATP, Adenosine triphosphate; FITC, Fluorescein Isothiocyanate; PI, propidium iodide; Bax, Bcl-2-associated X protein; Bcl-2, B-cell lymphoma-2; PARP, Poly (ADP-ribose) polymerase; DFO, Deferoxamine; Fer-1, Ferrostatin-1; BODIPY, 4,4-difluoro-3a,4a-diaza-s-indacene.

* Corresponding authors.
E-mail addresses: yerr@mail2.sysu.edu.cn (R.-R. Ye), rongtaolikm@163.com (R.-T. Li).
[1] These authors contributed equally.

https://doi.org/10.1016/j.jinorgbio.2021.111537
Received 16 February 2021; Received in revised form 24 June 2021; Accepted 5 July 2021
Available online 9 July 2021

Drugs with a single anticancer mechanism are usually not effective in treating tumors and are prone to drug resistance attributed to the polygenicity and complexity of cancer [17]. It has been reported that the development of anticancer agents with multiple action mechanisms can conquer these side effects and drug resistance [18]. Currently, the conjugation of organic molecules with anticancer potential and metal complexes has been demonstrated to be a promising strategy for developing anticancer agents with multiple action mechanisms. Moreover, metal complexes generally show superior biological activity than organic ligands, thus combining two of them may exert a synergistic effect [19,20]. Chen et al. reported two copper(II) complexes with isoquinoline derivatives as ligands to induce apoptosis and autophagy in human lung carcinoma (A549) [21]. Mao and Tan et al. prepared rhenium(I) complexes mixed with clinical iron chelator deferasirox to simultaneously disrupt mitochondrial metabolism and iron homeostasis [22]. Artesunate (ART), a chemical derivative of artemisinin, exerts diverse antitumor effects, such as antiproliferative, cell cycle regulation, and pro-apoptosis [23]. Recently, we reported a series of cyclometalated iridium(III) complexes incorporating ART, which exhibited synergistic anti-hepatocellular cancer activity [24].

Apoptosis is the classic cell death pathway that causes most of regulated cell death (RCD) in mammalian cells [25,26]. In addition, several regulated non-apoptotic cell death pathways have been recognized, such as autophagy, necroptosis, ferroptosis, etc. [27]. Ferroptosis, which plays a key role in a variety of organic diseases, especially cancer, is induced by the cumulation of lipid reactive oxygen species (ROS) mediated by the incapacitation of cellular GSH-dependent antioxidant defenses [28]. As the main source of ROS, mitochondria play a role in this type of RCD [29–31]. In addition, malondialdehyde (MDA), a lipid peroxidation marker, reflects the lipid peroxidation status [32]. The consumption of GSH and the suppression of glutathione peroxidase 4 (GPX4) are implicated in ferroptosis [33,34]. Thus, MDA level, cellular GSH and GPX4 expression are the hallmarks of ferroptosis formation. Until now, only a few metal-based complexes have been reported to cause cancer cell death through ferroptosis, including cisplatin [25], iridium(III) complex [35], and iron(III) complex [36]. Moreover, it is also pertinent to note that ART has been reported to have a ferroptosis-inducing effect [37].

Herein, two ART conjugated phosphorescent rhenium(I) complexes (Re(I)-ART conjugates), [Re(N^N)(CO)$_3$(PyCH$_2$OART)](PF$_6$) (**Re-ART-1** and **Re-ART-2**) (Scheme 1; Py = pyridine, N^N = 1,10-phenanthroline (phen, in **Re-ART-1**) and 4,7-diphenyl-1,10-phenanthroline (DIP, in **Re-ART-2**)) were designed and synthesized. The corresponding reference complexes [Re(phen)(CO)$_3$(PyCH$_2$OH)](PF$_6$) (**Re-1**) and [Re(DIP)(CO)$_3$(PyCH$_2$OH)](PF$_6$) (**Re-2**) that lack the ART group were also included. As the multi-faceted regulators of cell death, mitochondria are an important target for the development of anti-tumor drugs [38]. It has been reported that phosphorescent rhenium(I) complexes with high lipophilicity can preferentially accumulate in mitochondria [15,16,39]. According to our previous research findings, the introduction of an ART group can enhance the lipophilicity of cyclometalated iridium(III) complexes [24]. In this work, the ART group is expected to improve the lipophilicity of rhenium(I) complexes and further potentiate the mitochondrial targeting ability as well as synergistic anti-tumor activity of Re(I)-ART conjugates. In this study, we describe the synthesis, characterization, photophysical properties, and anticancer activity of Re(I)-ART conjugates as well as the anticancer mechanisms of **Re-ART-1** and **Re-ART-2**. Based on our findings, Re(I)-ART conjugates localize in mitochondria and induce mitochondrial dysfunction, thereby causing human cervical carcinoma (HeLa) cell death through a dual-mode of apoptosis and ferroptosis.

2. Results and discussion

2.1. Synthesis, photophysical characterization

The reference complex **Re-1** was synthesized according to the reference [40], and **Re-2** was obtained by a synthesis method similar to that of **Re-1**. The Re(I)-ART conjugates, **Re-ART-1** and **Re-ART-2**, were obtained through the condensation reaction of **Re-1** or **Re-2** with ART in anhydrous CH_2Cl_2 at room temperature using dicyclohexylcarbodiimide (DCC) as the dehydrating agent and 4-*N*,*N*-dimethylaminopyridine (DMAP) as the catalyst (Scheme S1). The products were purified with silica column chromatography (100:1 CH_2Cl_2:CH_3OH) and characterized using ESI-MS, ^{1}H NMR (Figs. S1-S6), and elemental analysis.

The electronic absorption and emission spectra of **Re-ART-1** and **Re-**

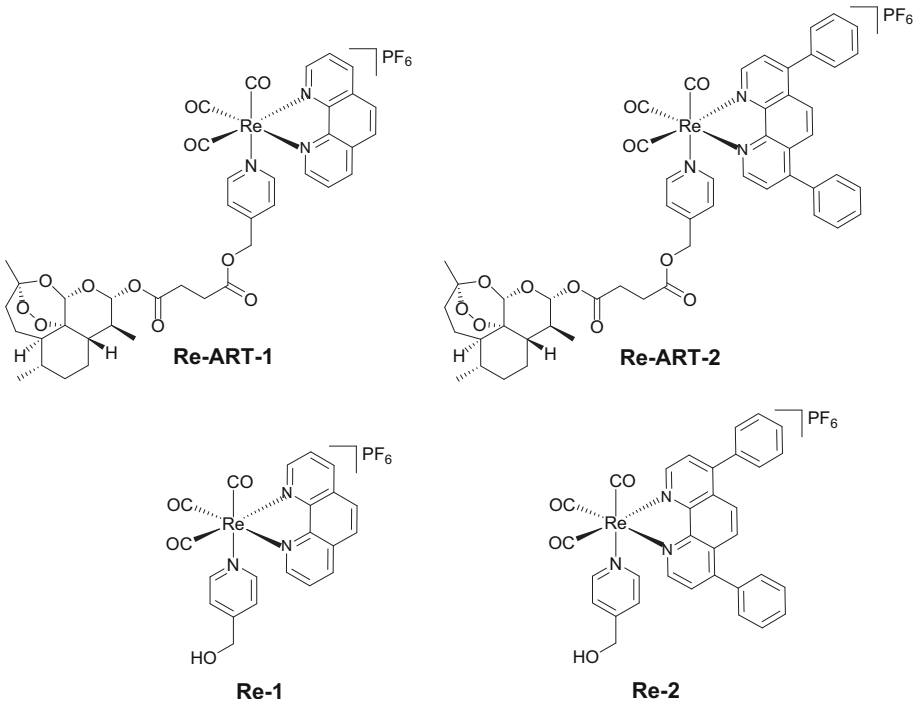

Scheme 1. Chemical structures of rhenium(I) complexes with (**Re-ART-1** and **Re-ART-2**) or without (**Re-1** and **Re-2**) ART.

ART-2 are shown in Fig. S7A. Re(I) complexes display two main bands at 250–450 nm in the case of the intraligand and metal-to-ligand charge-transfer transitions. After excitation at 405 nm, **Re-ART-1** and **Re-ART-2** emitted yellow light with a maximum wavelength of around 580 nm (Fig. S7B). The photophysical data of **Re-ART-1** and **Re-ART-2** are summarized in Table S1.

We further explored the stability of **Re-ART-1–2** in PBS by fluorescence spectroscopy and high performance liquid chromatography (HPLC). As shown in Fig. S8 and Fig. S9, no significant changes in the emission intensities and HPLC signals of **Re-ART-1**–**2** are observed, indicating the stability in PBS. Then, the responses of **Re-ART-1**–**2** towards esterase were monitored by fluorescence spectra. Porcine liver esterase (PLE) was used as a model to investigate the hydrolytic process of ester bonds in **Re-ART-1–2**. As shown in Fig. S10, the emission spectra of **Re-ART-1** display increased intensities upon treatment with PLE, while the spectra of **Re-ART-2** show decreased intensities. These results indicate that **Re-ART-1**–**2** can undergo hydrolysis in the presence of esterase.

2.2. Lipophilicity and in vitro cytotoxicity

The cellular uptake, distribution and cytotoxicity of metal-based complexes are strongly affected by their lipophilicity (log $P_{o/w}$) [41]. It has been reported that a molecule with a log $P_{o/w}$ value between 0 and + 5 and a cation number more than 0 shows a high probability to localize in mitochondria [42]. Therefore, we used the shake flask method to determine the lipophilicity of Re(I) complexes. The log $P_{o/w}$ values are listed in the following order: **Re-1** (0.66) < **Re-ART-1** (1.08) < **Re-2** (1.54) < **Re-ART-2** (1.96), which reveals that the conjugation of ART can enhance the lipophilicity of Re(I) complexes.

As rhenium is an exogenous element, the quantitative measurement of the cellular uptake levels of Re(I) complexes was studied by inductively coupled plasma mass spectrometry (ICP-MS) measurement. Upon incubation with 10 μM Re(I) complexes on HeLa cells for 1 h, the intracellular rhenium contents of the compounds are in the following order: **Re-ART-2** (2013.4 ng/10^6 cells) > **Re-2** (1043.2 ng/10^6 cells) > **Re-ART-1** (847.3 ng/10^6 cells) > **Re-1** (278.7 ng/10^6 cells). Thus, the cellular uptake efficiency of Re(I) complexes is well correlated with their lipophilicities.

The antiproliferative effects of **Re-ART-1** and **Re-ART-2** were tested against HeLa, A549, A549R (cisplatin-resistant A549), HepG2 (human hepatocellular liver carcinoma) and LO2 (human normal liver) cells. For comparison, **Re-1**, **Re-2**, ART, the mixtures of **Re-1/2** with ART (**Re-1** + ART, **Re-2** + ART) and cisplatin were included. According to the IC_{50} values in Table 1, the antiproliferative effects of the compounds are as follows: ART < **Re-1** ≈ **Re-1** + ART < cisplatin < **Re-ART-1** < **Re-2** ≈ **Re-2** + ART < **Re-ART-2**, which are unanimous with their lipophilicity. **Re-ART-2**, with IC_{50} values ranging from 0.8–1.5 μM, is the most potent among all tested compounds. Coupling with ART can significantly improve the cytotoxicity of rhenium(I) complexes, whereby **Re-ART-1** and **Re-ART-2** showed about 4.5- to 12.2-fold higher cytotoxicity than **Re-1** and **Re-2** against the tested human cancer cell lines. In addition, **Re-ART-1** and **Re-ART-2** display approximately 3.9- to 57.6-fold greater ability to kill A549R cells than cisplatin, indicating that they can conquer the resistance of cisplatin. Furthermore, the cytotoxicity of **Re-ART-1** and **Re-ART-2** against LO2 cells was determined to be approximately 2.0- to 8.6-fold lower than that of HepG2 cells, revealing their selectivity to cancer cells.

Table 1
IC_{50} values of tested compounds towards different cell lines[a].

Compound	IC_{50} (μM)				
	HeLa	A549	A549R	HepG2	LO2
Re-ART-1	5.2 ± 0.5	13.2 ± 1.7	21.9 ± 2.5	11.4 ± 1.2	22.4 ± 3.0
Re-ART-2	0.8 ± 0.1	1.1 ± 0.2	1.5 ± 0.2	1.0 ± 0.1	8.6 ± 1.1
Re-1	63.8 ± 0.7	79.8 ± 4.2	> 100	91.9 ± 2.5	> 100
Re-2	4.8 ± 0.2	5.1 ± 0.3	6.7 ± 0.5	5.5 ± 1.1	8.8 ± 0.8
Re-1 + ART	59.1 ± 1.7	62.4 ± 5.8	87.8 ± 5.2	85.4 ± 1.8	85.3 ± 2.1
Re-2 + ART	4.9 ± 0.6	4.6 ± 0.3	5.4 ± 1.0	5.4 ± 0.4	6.0 ± 1.6
ART	> 100	> 100	> 100	> 100	> 100
cisplatin	20.0 ± 2.1	18.2 ± 1.5	86.5 ± 9.0	22.4 ± 2.0	30.5 ± 2.8

[a] IC_{50} values are drug concentrations necessary for 50% inhibition of cell viability. The data are presented as mean ± standard deviation (SD) and cell viability is assessed after 48 h incubation.

2.3. Cellular localization and uptake mechanisms

Since the anticancer mechanism of metal-based complexes is closely related to their cellular localization [16], the cellular uptake and intracellular distribution of **Re-ART-1** and **Re-ART-2** were investigated by confocal microscopy. As shown in Fig. S11, both compounds can effectively penetrate HeLa cells and exhibit blatant organelle staining. Further co-localization study demonstrates that the fluorescence of **Re-ART-1** and **Re-ART-2** overlays with that of MitoTracker Deep Red FM (MTDR) (Fig. 1A), however, almost no overlap was observed with the fluorescence of LysoTracker Deep Red FM (LTDR) (Fig. 1B). The Pearson's correlation coefficients of **Re-ART-1** and **Re-ART-2** with MTDR are 0.83 and 0.91, respectively. These data display that Re(I)-ART conjugates are primarily distributed in mitochondria.

The pathways for small molecules to penetrate cells mainly include energy-dependent and energy-independent [43]. To evaluate the entry of the complexes into cells, we studied the cellular uptake mechanisms of **Re-ART-1** and **Re-ART-2**. HeLa cells were pre-treated under different conditions and then incubated with Re(I)-ART conjugates (10 μM) for 1 h. Compared to that at 37 °C, the suppressed cellular luminescence was observed when treated with **Re-ART-1** and **Re-ART-2** at 4 °C or pre-treated with the metabolic inhibitor cyanide 3-chlorophenylhydrazone (CCCP) (Fig. 2). However, the cellular luminescence was barely influenced for pre-treated HeLa cells with endocytic inhibitor chloroquine. This result means that Re(I)-ART conjugates are taken up through the energy-dependent mechanism instead of endocytic pathways.

2.4. Mitochondrial damage

Mitochondrial integrity can be reflected by the mitochondrial membrane potential (MMP) [44]. As **Re-ART-1** and **Re-ART-2** mainly accumulate in mitochondria, their impact on MMP was examined by confocal microscopy using rhodamine 123 (Rh123) staining. Rh123 is an MMP-dependent fluorescent probe, a decrease in fluorescence intensity of Rh123 can indicate the loss of MMP [45]. After treating HeLa cells with different doses of **Re-ART-1** or **Re-ART-2** for 6 h, the fluorescence intensity of Rh123 decreased in a concentration-dependent manner (Fig. 3), indicating the loss of MMP.

Mitochondria are the main organelles for cellular energy production, as a result of the loss of MMP, cellular adenosine triphosphate (ATP) levels should be disturbed [46]. The impact of Re(I)-ART conjugates on cellular ATP levels was measured, using **Re-1**–**2** as controls. As shown in Fig. 4, the intracellular ATP levels decreased in a concentration-dependent manner after treating HeLa cells with Re(I) complexes for 6 h, while **Re-ART-1**–**2** performed better than **Re-1**–**2** at the same concentration. Notably, compared with the control, treatment of HeLa cells with 12.5 μM **Re-ART-1** or **Re-ART-2** reduced the intracellular ATP levels to 40.5% (**Re-ART-1**) and 19.9% (**Re-ART-2**), respectively. The results imply that Re(I)-ART conjugates can cause the dysfunction of mitochondria.

2.5. Elevation of intracellular ROS levels

In addition to energy production, mitochondria are also the main site of ROS production [47]. It has been reported that the loss of MMP is

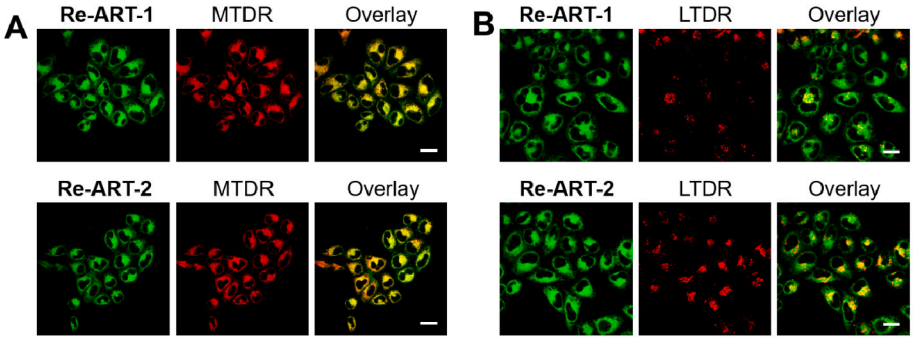

Fig. 1. The colocalization assay of Re(I)-ART conjugates (10 μM) with MTDR (150 nM) (A) or LTDR (50 nM) (B) (Re(I)-ART conjugates: λ_{ex} = 405 nm, λ_{em} = 560 ± 20 nm; MTDR and LTDR: λ_{ex} = 633 nm, λ_{em} = 665 ± 20 nm). Scale bar: 20 μm.

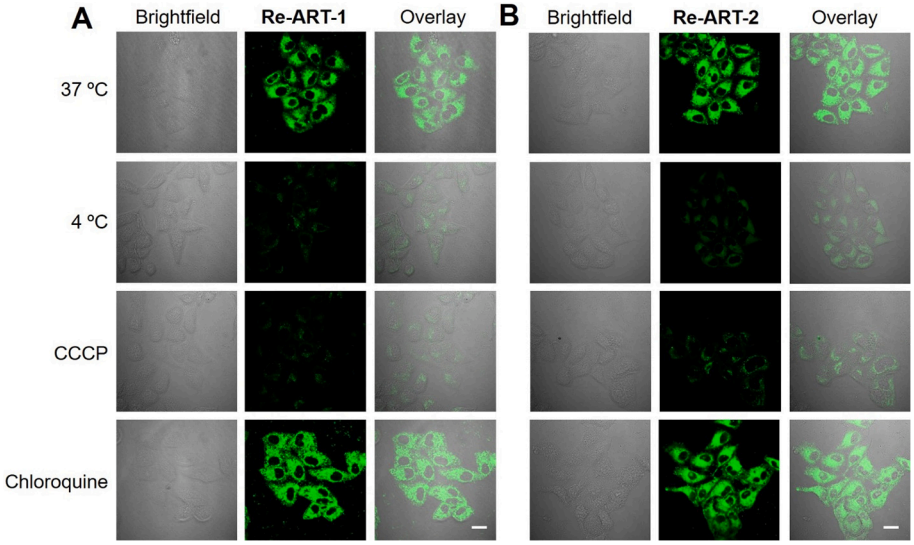

Fig. 2. Cellular uptake mechanisms of Re(I)-ART conjugates. HeLa cells were incubated with Re(I)-ART conjugates (10 μM) under different temperatures (37 °C and 4 °C), pre-treated with CCCP (30 μM) or chloroquine (50 μM) (λ_{ex} = 405 nm, λ_{em} = 560 ± 20 nm). Scale bar: 20 μm.

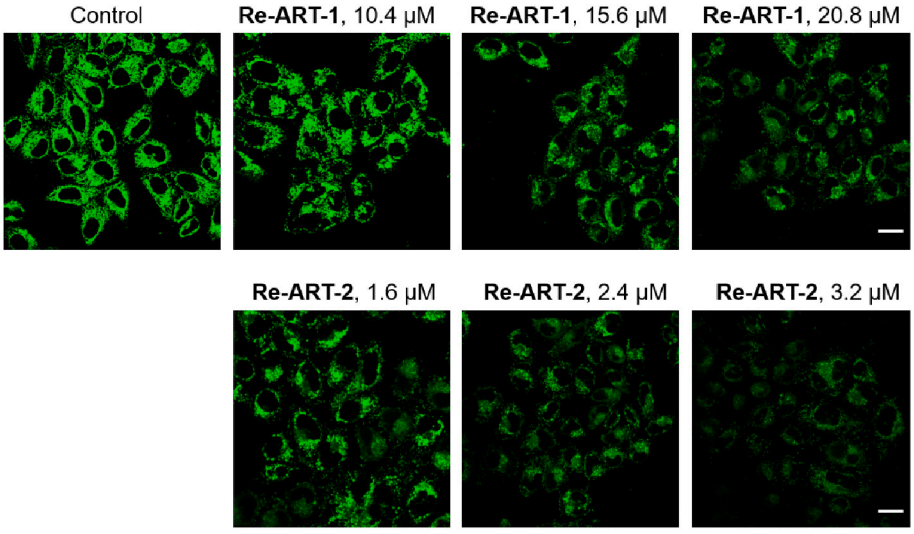

Fig. 3. Re(I)-ART-induced the loss of MMP analyzed by confocal microscopy with Rh123 staining (λ_{ex} = 488 nm, λ_{em} = 530 ± 20 nm). Scale bar: 20 μm.

closely related to the increase of intracellular ROS [48]. ART [49] or rhenium(I) complexes [15,16] can induce the elevation of ROS levels. Herein, the intracellular ROS-accumulating capability of **Re-ART-1** and **Re-ART-2** was detected by staining with 2′,7′-dichlorodihydrouorescein diacetate (H_2DCFDA). H_2DCFDA is non-fluorescent and can be oxidized by intracellular ROS to highly fluorescent 2′,7′-dichlorofluorescein

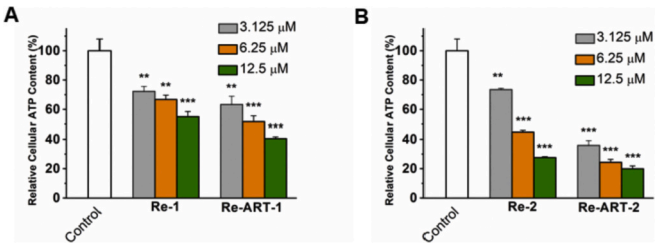

Fig. 4. ATP levels in HeLa cells treated with different concentrations of Re(I) complexes (* compared with control, * $P < 0.05$, ** $P < 0.01$, *** $P < 0.001$).

(DCF) [50]. As shown in Fig. 5, treating HeLa cells with **Re-ART-1** or **Re-ART-2** caused a concentration-dependent increase in DCF fluorescence intensity, indicating the elevation of ROS.

2.6. Induction of apoptosis

Mitochondria are important players in controlling the intrinsic pathway of apoptosis [51]. Mitochondrial damage and ROS accumulation are two important phenomena of apoptosis, we tested the ability of Re(I)-ART conjugates to induce apoptosis. As shown in Fig. 6, HeLa cells treated with **Re-ART-1** and **Re-ART-2** exhibited typical changes in apoptotic morphology (such as cell shrinkage and nuclear fragmentation) in a concentration-dependent manner. Moreover, annexin V-FITC/PI (FITC: fluorescein isothiocyanate; PI: propidium iodide) double staining analysis demonstrated that HeLa cells treated with **Re-ART-1** or **Re-ART-2** for 24 h increased the percentage of apoptotic cells in a concentration-dependent manner (Fig. 7). Specifically, treatment with **Re-ART-1** (20.8 μM) or **Re-ART-2** (3.2 μM) significantly increased the percentage of apoptotic cells from 2.75% (control) to 29.30% (**Re-ART-1**) and 32.22% (**Re-ART-2**), respectively. Overall, the results indicate that Re(I)-ART conjugates can induce HeLa cell apoptosis.

To further investigate the apoptotic mechanism induced by Re(I)-ART conjugates, we examined the changes in Bcl-2-associated X protein (Bax), B-cell lymphoma-2 (Bcl-2), caspase-3, and Poly (ADP-ribose) polymerase (PARP) expression. The Bcl-2 family contains both pro-apoptotic protein Bax and anti-apoptotic protein Bcl-2. During apoptosis, Bax undergoes translocation from the cytoplasm to mitochondria, changes its conformation, triggers the emancipation of cytochrome C, and participates in the caspase activation pathway associated with mitochondria [52]. PARP is an important biochemical marker for testing apoptosis [53]. As a member of the cysteine protease family, caspase-3 facilitates the cleavage of PARP in the execution phase of apoptosis [54]. As shown in Fig. 8, **Re-ART-1** and **Re-ART-2** markedly up-regulated the expression of Bax and down-regulated the expression of Bcl-2. Moreover, **Re-ART-1** and **Re-ART-2** also induced the cleavage of caspase-3 and PARP in a dose-dependent manner. These data indicate that Re(I)-ART conjugates induce the apoptosis of HeLa cells through a caspase-dependent pathway.

2.7. Induction of ferroptosis

The abnormal increase of intracellular ROS is closely related to apoptosis and ferroptosis [55,56]. Ferroptosis, which is controlled by iron-dependent lipid hydroperoxides accumulation [27], can be inhibited by antioxidant ferrostatin-1 (Fer-1) or iron chelators (e.g., deferoxamine (DFO)) [57]. **Re-ART-1** and **Re-ART-2** were proved their ability to induce apoptosis. To examine whether the occurrence of ferroptosis was involved in HeLa cell death induced by Re(I)-ART conjugates, we investigated the effects of **Re-ART-1** and **Re-ART-2** each concomitantly incubated with DFO and Fer-1 on the viability of HeLa cells, using **Re-1**–**2** as controls. As shown in Fig. 9A, B and Fig. S12, compared with cells treated with Re(I) complexes alone, cells treated with DFO and Fer-1 exhibited an increase in cell viability, except for **Re-1**. As for DFO, the viability of HeLa cells increased 1.7-fold for **Re-2**, 1.8-fold for **Re-ART-1**, and 2.5-fold for **Re-ART-2**. As for Fer-1, the viability of HeLa cells increased 1.7-fold for **Re-2**, 1.9-fold for **Re-ART-1**, and 2.6-fold for **Re-ART-2**. The results partially indicate that **Re-2** and **Re-ART-1**–**2** can induce ferroptosis, whereby **Re-ART-1**–**2** exhibit a better ferroptosis inducing ability than **Re-1**–**2**.

GPX4 is important in preventing lipid peroxidation, which is inactivated by the depletion of GSH, thus inducing ferroptosis [34,58,59]. Accordingly, we further measured the depletion of GSH in HeLa cells. As shown in Fig. 9C, HeLa cells treated with **Re-ART-1** and **Re-ART-2** significantly reduced the GSH levels in a concentration-dependent manner. The influence of **Re-ART-1** and **Re-ART-2** on the expression of GPX4 was also examined. As shown in Fig. 9D, HeLa cells treated with **Re-ART-1** and **Re-ART-2** remarkably decreased the levels of GPX4 expression in a concentration-dependent manner. It has been reported the suppression of GPX4 activity can lead to intracellular lipid peroxidation accumulation, which is an important indicator of ferroptosis [60]. Therefore, the influence of **Re-ART-1** and **Re-ART-2** on lipid peroxidation was also assessed by measuring the levels of MDA. As shown in Fig. 9E, treated HeLa cells with **Re-ART-1** or **Re-ART-2**

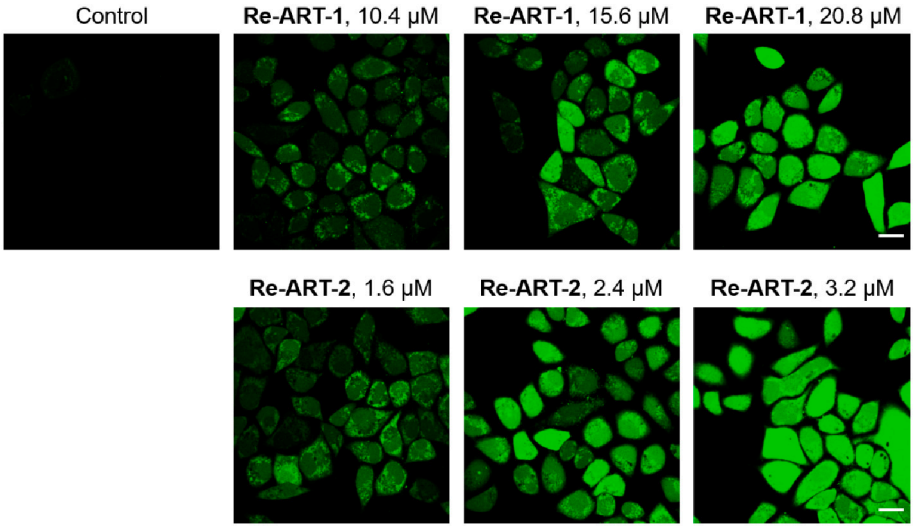

Fig. 5. Re(I)-ART-induced the elevation of intracellular ROS levels examined by confocal microscopy with H_2DCFDA staining ($\lambda_{ex} = 488$ nm, $\lambda_{em} = 530 \pm 20$ nm). Scale bar: 20 μm.

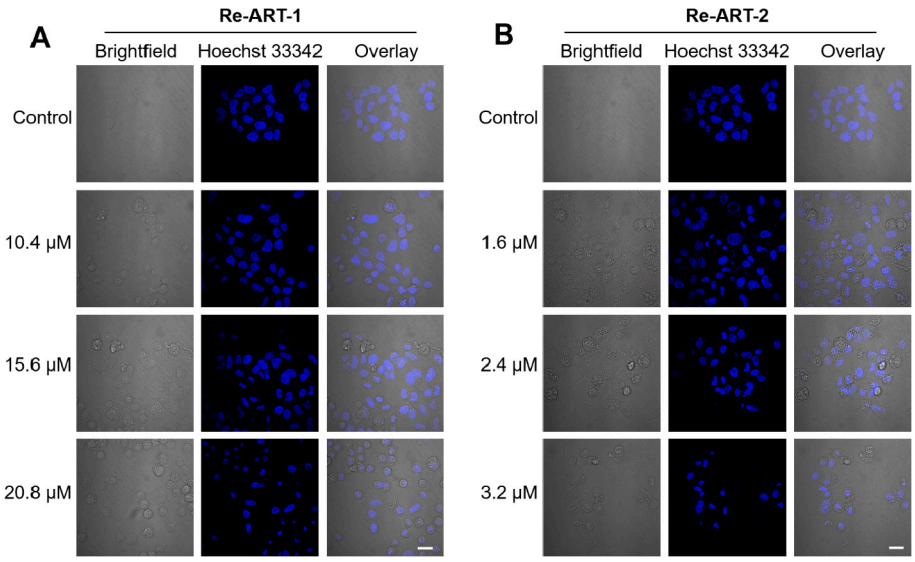

Fig. 6. Re(I)-ART-induced HeLa cells apoptosis measured by confocal microscopy with Hoechst 33342 staining (λ_{ex} = 405 nm, λ_{em} = 460 ± 20 nm). Scale bar: 20 μm.

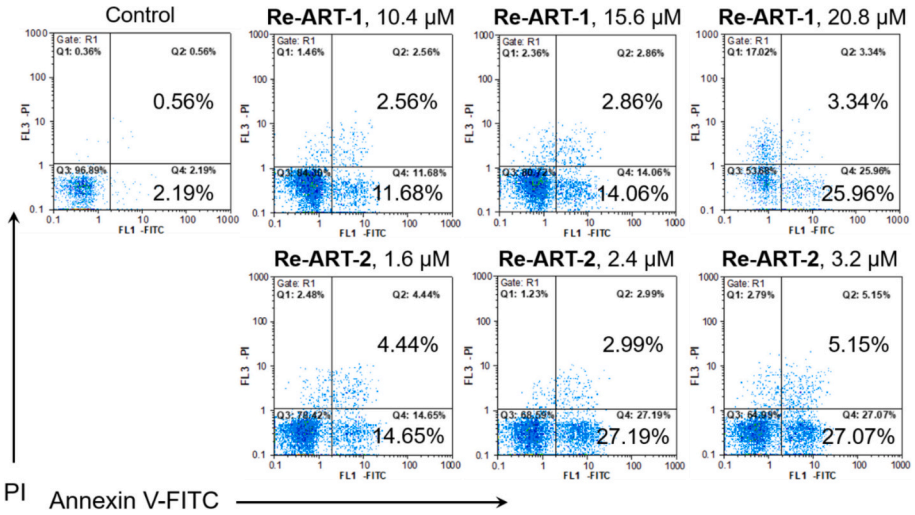

Fig. 7. Re(I)-ART-induced HeLa cells apoptosis measured by flow cytometry with Annexin V-FITC/PI staining.

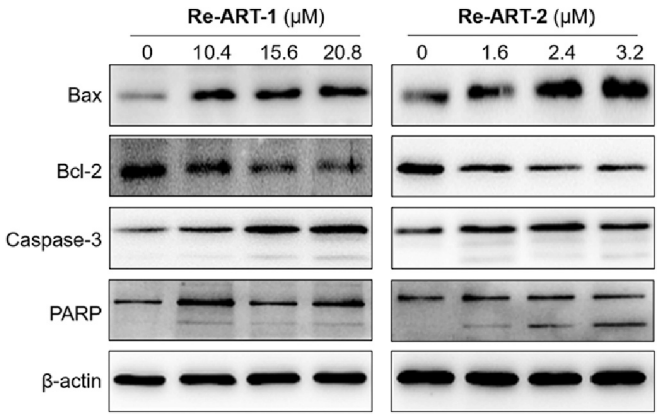

Fig. 8. Expression of apoptosis-related protein (Bax, Bcl-2, caspase-3 and PARP) in HeLa cells treated with Re(I)-ART conjugates.

exhibited a dose-dependent increase in MDA levels. Particularly, cells treated with 3.2 μM **Re-ART-2** showed a more than 8.5-fold increase in MDA levels. Lipid peroxidation was further measured using a lipid peroxidation-sensitive dye C11-BODIPY (4,4-difluoro-3a,4a-diaza-s-indacene) 581/591. The red fluorescence is representative of non-oxidized lipids in cells labelled with C11-BODIPY 581/591, while the green fluorescence represents oxidized lipids. As shown in Fig. 10, HeLa cells in the **Re-ART-1**–**2** groups show the strongest green fluorescence in confocal images compared to those of cells in the other groups. Flow cytometric assay also confirms that **Re-ART-1**–**2** induced lipid peroxide accumulation (Fig. S13). These results collectively demonstrate that Re(I)-ART conjugates inhibit the GPX4 pathway and induce lipid peroxidation accumulation, leading to ferroptosis.

3. Conclusions

In summary, we have developed two ART conjugated phosphorescent rhenium(I) complexes, **Re-ART-1** and **Re-ART-2**, with dual anticancer mechanisms. These two complexes display high cytotoxicity towards human tumor cells. Cellular uptake experiments reveal that **Re-ART-1** and **Re-ART-2** can effectively target mitochondria. Mechanistic

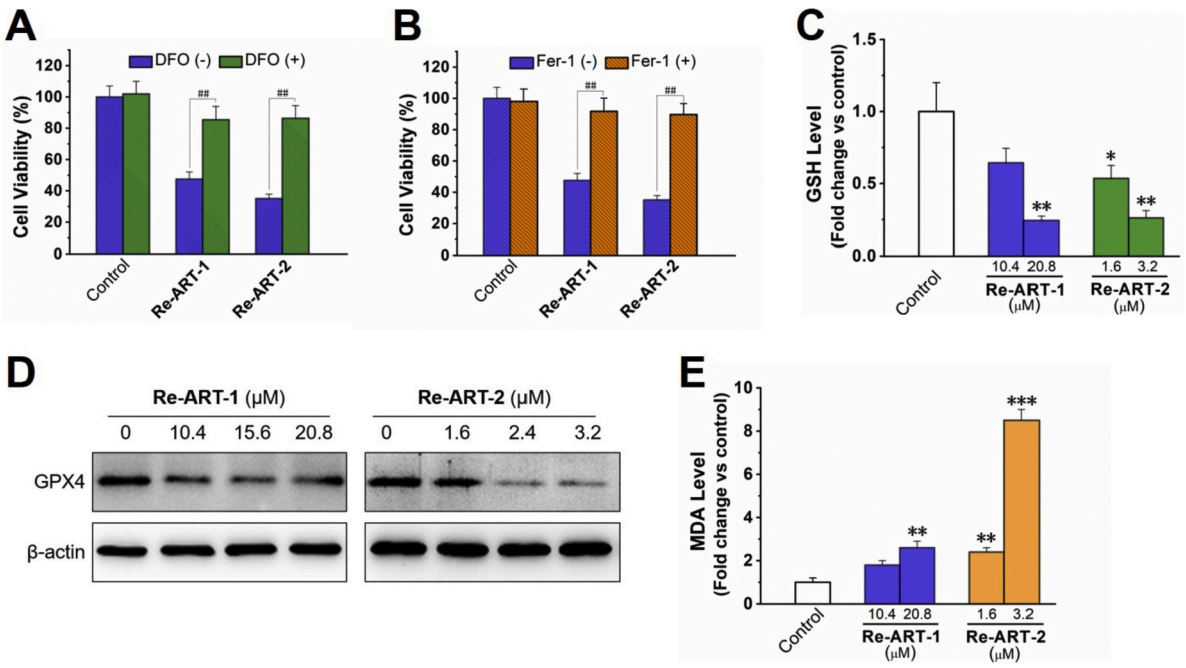

Fig. 9. The ferroptosis induced by Re(I)-ART conjugates in HeLa cells. The effects of **Re-ART-1** and **Re-ART-2** each concomitantly incubated with DFO (100 μM) (A) and Fer-1 (100 nM) (B) on the viability of HeLa cells. GSH level (C), expression of GPX4 (D) and MDA level (E) in HeLa cells treated with **Re-ART-1** and **Re-ART-2** (* compared with control, * $P < 0.05$, ** $P < 0.01$, *** $P < 0.001$; # Fer-1 (−)/DFO (−) compared with Fer-1 (+)/DFO (+), # $P < 0.05$, ## $P < 0.01$, ### $P < 0.001$).

studies indicate that **Re-ART-1** and **Re-ART-2** can induce apoptosis through the depolarization of MMP, consumption of cellular ATP, elevation of ROS and caspase cascade. Furthermore, **Re-ART-1** and **Re-ART-2** can inhibit the GPX4 pathway and induce lipid peroxidation accumulation, thus leading to ferroptosis. Overall, these Re(I)-ART conjugates show promising application as synergetic anticancer agents, which can induce a dual-killing mode of apoptosis-ferroptosis to enhance cancer therapy.

4. Experimental section

4.1. Materials and instruments

$Re(CO)_5Cl$ (Sigma Aldrich), phen (J&K), DIP (J&K), $PyCH_2OH$ (J&K), ART (Alfa Aesar), DCC (Alfa Aesar), DMAP (Alfa Aesar), NH_4PF_6 (Alfa Aesar), Dulbecco's Modified Eagle Medium (DMEM, Gibco), fetal bovine serum (FBS, Gibco), penicillin-streptomycin (Gibco), 3-(4,5-dimethylthiazol-2-yl)-2,5-diphenyltetrazolium bromide (MTT) (J&K), CCCP (J&K), chloroquine (J&K), Rh123 (J&K), H_2DCFDA (J&K), Hoechst 33342 (J&K), Fer-1 (J&K), DFO (J&K). Annexin V-FITC Apoptosis Detection Kit, GSH and GSSG (oxidized glutathione) Assay Kit and MDA Assay Kit were purchased from Beyotime (Jiangsu, China). Primary antibodies against Bax, Bcl-2, caspase-3, PARP and GPX4 were purchased from Cell Signaling Technology. **Re-ART-1**, **Re-ART-2**, **Re-1**, **Re-2** and ART were dissolved in dimethyl sulfoxide (DMSO) just before the experiments, and the concentration of DMSO in biological experiments was 1% (*v*/v). Cisplatin was dissolved in 0.9% sodium chloride solution just before use.

A LCQ DECA XP spectrometer was used for obtaining ESI-MS spectra. A Bruker Avance 600 spectrometer was used for obtaining ^{1}H NMR spectra. A SpetraMax M2 plate reader was used for determining cell viability. A Nikon A1R/A1 laser-scanning confocal microscope was used for obtaining cell imaging images. A CyFlow Space flow cytometer was used for performing the flow cytometry analysis.

4.2. Preparation of rhenium(I) complexes

$Re(phen)(CO)_3Cl$ [61], $Re(DIP)(CO)_3Cl$ [62] and $[Re(phen)(CO)_3(PyCH_2OH)](PF_6)$ (**Re-1**) [40] were synthesized following the literature procedures.

$[Re(DIP)(CO)_3(PyCH_2OH)](PF_6)$ (**Re-2**): The preparation of **Re-2** was similar to that of **Re-1** except that $Re(DIP)(CO)_3Cl$ was used instead of $Re(phen)(CO)_3Cl$. Yield: 0.250 g (orange powder), 85%. ^{1}H NMR (600 MHz, [D_6]DMSO) δ 9.84 (d, $J = 5.4$ Hz, 2H), 8.54 (d, $J = 5.4$ Hz, 2H), 8.23 (d, $J = 5.4$ Hz, 2H), 8.16 (s, 2H), 7.73–7.68 (m, 10H), 7.33 (d, $J = 5.6$ Hz, 2H), 5.53 (s, 1H), 4.46 (d, $J = 5.4$ Hz, 2H). ESI-MS (CH_3OH): *m/z* 712 $[M - PF_6]^+$. Elemental analysis: calcd (%) for $C_{33}H_{23}F_6N_3O_4PRe$: C, 46.26; H, 2.71; N, 4.90; found: C, 46.56; H, 2.87; N, 4.79.

Re-ART-1: The synthetic route of **Re-ART-1** was shown in Scheme S1. Firstly, the mixture of ART (10 equiv.), DCC (1.5 equiv.) and DMAP (1.5 equiv.) were stirred in dry CH_2Cl_2 for 30 min, and then **Re-1** (1 equiv.) in dry CH_2Cl_2 was added drop-wise. After stirring the mixture at ambient temperature for 24 h, the solvent was evaporated. The crude product was purified using column chromatography on silica gel by elution with CH_2Cl_2/CH_3OH (100:1). Yield: 0.223 g (orange powder), 70%. ^{1}H NMR (600 MHz, [D_6]DMSO) δ 9.77 (d, $J = 5.1$ Hz, 2H), 9.05 (d, $J = 8.3$ Hz, 2H), 8.44 (d, $J = 6.3$ Hz, 2H), 8.32 (s, 2H), 8.28–8.24 (m, 2H), 7.28 (d, $J = 5.8$ Hz, 2H), 5.60 (d, $J = 9.7$ Hz, 1H), 5.52 (s, 1H), 5.03 (s, 2H), 2.64 (s, 4H), 2.24–2.13 (m, 2H), 1.99 (dd, $J = 13.9$, 2.4 Hz, 1H), 1.84–1.79 (m, 1H), 1.62–1.56 (m, 2H), 1.54–1.50 (m, 1H), 1.41 (dt, $J = 13.1$, 6.5 Hz, 2H), 1.33–1.27 (m, 1H), 1.22 (s, 3H), 1.20–1.14 (m, 1H), 0.99–0.92 (m, 1H), 0.89 (d, $J = 6.2$ Hz, 3H), 0.63 (d, $J = 7.1$ Hz, 3H). ESI-MS (CH_3OH): *m/z* 926.2315 $[M - PF_6]^+$. Elemental analysis: calcd (%) for $C_{40}H_{41}F_6N_3O_{11}PRe$: C, 44.86; H, 3.86 N, 3.92; found: C, 44.56; H, 3.89; N, 3.79.

Re-ART-2: Complex **Re-ART-2** was prepared following a similar procedure to that of **Re-ART-1** except that **Re-2** was used instead of **Re-1**. Yield: 0.258 g (brown powder), 75%. ^{1}H NMR (600 MHz, [D_6]DMSO) δ 9.84 (d, $J = 5.3$ Hz, 2H), 8.60 (d, $J = 5.3$ Hz, 2H), 8.22 (t, $J = 4.9$ Hz, 2H), 8.17 (s, 2H), 7.74–7.67 (m, 10H), 7.37 (d, $J = 5.3$ Hz, 2H), 5.61 (d, $J = 9.8$ Hz, 1H), 5.52 (s, 1H), 5.10 (s, 2H), 2.66 (s, 4H), 2.24–2.13 (m,

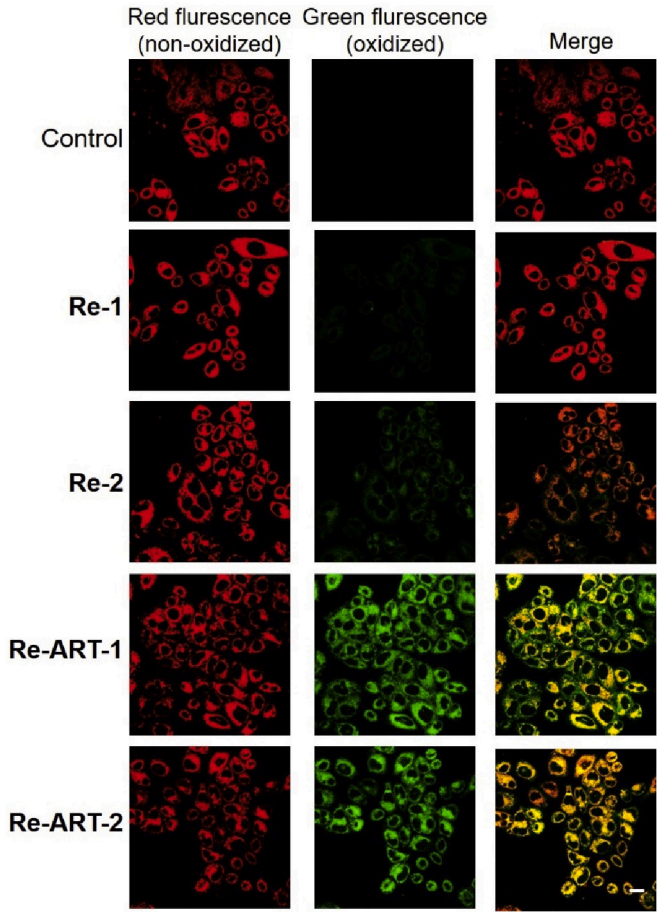

Fig. 10. Confocal imaging of HeLa cells incubated with Re(I) complexes (4 × IC_{50}, 6 h) via C11-BODIPY 581/591 staining (λ_{ex} = 488 nm, λ_{em} = 510 ± 20 nm (green); λ_{ex} = 581 nm, λ_{em} = 591 ± 20 nm (red)). Scale bar: 20 μm. (For interpretation of the references to colour in this figure legend, the reader is referred to the web version of this article.)

2H), 2.01–1.96 (m, 1H), 1.83–1.78 (m, 1H), 1.59–1.54 (m, 2H), 1.49 (dd, *J* = 10.8, 6.7 Hz, 1H), 1.42–1.36 (m, 2H), 1.33–1.28 (m, 1H), 1.22 (s, 3H), 1.18–1.14 (m, 1H), 1.10 (d, *J* = 7.0 Hz, 1H), 0.88 (d, *J* = 6.4 Hz, 3H), 0.64 (d, *J* = 7.0 Hz, 3H). ESI-MS (CH_3OH): *m/z* 1078.2942 $[M - PF_6]^+$. Elemental analysis: calcd (%) for $C_{52}H_{49}F_6N_3O_{11}PRe$: C, 51.06; H, 4.04; N, 3.44; found: C, 51.17; H, 4.12; N, 3.43.

4.3. Stability analysis

The stability of **Re-ART-1–2** was determined using fluorescence spectra and HPLC. *Fluorescence spectra*: the stock solution (2×10^{-5} M) of complexes in PBS was prepared, and then divided them into two equal parts, respectively. The first part of the solution was measured immediately. The second part of the solution was kept for 48 h, and then monitored using fluorescence spectrophotometer. *HPLC*: **Re-ART-1–2** were dissolved in acetonitrile and detected with a UV detector set at 254 nm and a flow rate of 1 mL/min and a solvent system of MeOH-H_2O (75: 25).

4.4. Hydrolysis of Re(I)-ART complexes by PLE in vitro

Re(I) complexes (2×10^{-5} M) in PBS were freshly prepared in quartz cuvettes (3 mL), and then PLE (1 μL) was added. Time-dependent emission spectra were recorded after reaction for 5 min at 298 K.

4.5. Cell lines and culture conditions

HeLa, HepG2, A549, A549R and LO2 cells were purchased from Nanjing KeyGen Biotechnology Co., Ltd., and cultured in DMEM or RPMI 1640 complete medium at 37 °C with 5% CO_2 atmosphere.

4.6. Lipophilicity

The lipophilicity of rhenium(I) complexes is presented as log $P_{o/w}$ values, which were obtained from a previous study [63].

4.7. ICP-MS measurement

HeLa cells were seeded in 10 cm tissue culture dishes and incubated for 24 h. The medium was removed and replaced with fresh medium containing Re(I) complexes (10 μM). After 1 h incubation, the cells were washed with PBS, trypsinized and collected. The cells were counted and digested with HNO_3 (65%, 0.5 mL). The rhenium content in cells was determined by ICP-MS.

4.8. In vitro cytotoxicity assay

The anticancer activities of rhenium(I) complexes against HeLa, A549, A549R, HepG2 and LO2 cells were detected using MTT assay. The tested cells were placed in 96-well plates at a density of 5×10^4/well for 24 h at 37 °C. After replacing the culture medium with a fresh medium containing the Re(I) complexes with/without inhibitors (Fer-1 or DFO) at the indicated concentration, the cells were cultured at 37 °C for 48 h. Afterwards, MTT solution was added and co-incubated at 37 °C for an additional 4 h. Last, 150 μL/well DMSO was used to take over the media and dissolve the MTT-formazan crystals. A SpetraMax M2 plate reader was applied to detect the absorbance of living cells at 570 nm.

4.9. Cellular localization assay

HeLa cells (5×10^5/well) were seeded in a 35 mm glass-bottom cell culture dish overnight, then co-cultured with Re(I)-ART conjugates (10 μM) and MTDR (150 nM) or LTDR (50 nM) for 1 h. Subsequently, cells were immediately monitored by confocal microscopy. Excitation wavelength of Re(I)-ART conjugates was 405 nm and their emission wavelength was 560 ± 20 nm. For MTDR and LTDR, the excitation and emission wavelengths were 633 nm and 665 ± 20 nm, respectively.

4.10. Measurement of MMP

HeLa cells (5×10^5/well) were seeded in a 35 mm glass-bottom cell culture dish overnight. After incubating with Re(I)-ART conjugates for 6 h, HeLa cells were rinsed twice with PBS, then stained with Rh123 (1 μg/mL) for 30 min. After washing with PBS twice, cells were observed with confocal microscopy (λ_{ex} = 488 nm, λ_{em} = 530 ± 20 nm).

4.11. Intracellular ATP detection

The tested cells were placed in 96-well plates at a density of 5×10^4/well for 24 h at 37 °C. After incubating with Re(I)-ART conjugates for 6 h, the CellTiter-Glo® Luminescent Cell Viability Assay kit was used to measure the cellular ATP level following the manufacturer's manual.

4.12. Measurement of intracellular ROS

HeLa cells (5×10^5/well) were seeded in a 35 mm glass-bottom cell culture dish overnight. After incubating with Re(I)-ART conjugates for 6 h, HeLa cells were rinsed with serum-free DMEM twice, then labelled with H_2DCFDA (10 μM). Subsequently, cells were washed and examined under confocal microscopy (λ_{ex} = 488 nm, λ_{em} = 530 ± 20 nm).

4.13. Hoechst 33342 staining

HeLa cells (5×10^5/well) were seeded in a 35 mm glass-bottom cell culture dish overnight. After incubating with Re(I)-ART conjugates for 24 h, HeLa cells were fixed with 4% paraformaldehyde. Then, Hoechst 33342 (5 μg/mL) was used to label cells which were observed under confocal microscopy ($\lambda_{ex} = 405$ nm, $\lambda_{em} = 460 \pm 20$ nm).

4.14. Annexin V/PI staining

HeLa cells were seeded in 6-well plates at a density of 1×10^6/well and incubated for 24 h. After incubating with Re(I)-ART conjugates for 24 h, cells were collected and resuspended in 500 μL of binding buffer containing 5 μL annexin V and 10 μL PI. After 10 min of co-incubation in dark, flow cytometry was used to analyze cells ($\lambda_{ex} = 488$ nm, $\lambda_{em} = 530$ nm ± 20 nm (annexin V) and 620 ± 20 nm (PI)).

4.15. Western blot analysis

Bax, Bcl-2, caspase-3, PARP and GPX4 protein extracts were prepared from HeLa cells. Cells were seeded in 60 mm plates (2×10^6/well) and incubated overnight for cell attachment. After treating with different doses of Re(I)-ART conjugates for 24 h, cells were lysed, and lysates were centrifuged at 4 °C for 20 min. The protein concentration was determined using the BCA assay kit. Equal amounts of protein were ran on SDS-PAGE and then transferred to the PVDF membrane. After blocking for 2 h at r.t., membranes were first incubated with primary antibodies against Bax, Bcl-2, caspase-3, PARP and GPX4, then incubated with secondary antibodies.

4.16. Intracellular GSH measurement

A GSH and GSSG Assay Kit was used to detect intracellular GSH. HeLa cells were incubated with different doses of Re(I)-ART conjugates for 24 h. Afterwards, cells were lysed by the freeze-thaw method, and the lysate was centrifuged at 4 °C for 5 min to collect the supernatant. Then, the above supernatant (200 μL) was added to the test working solution and incubated together at r.t. for 2 min. The absorption of intracellular GSH at 405 nm was recorded by a SpetraMax M2 plate reader.

4.17. Intracellular MDA assay

After incubation with Re(I)-ART conjugates for 24 h, cells were lysed with the lysis buffer. Then, the lysate was centrifuged at 4 °C for 15 min to collect the supernatant. Lipid Peroxidation MDA assay kit was used to detect the MDA content.

4.18. Intracellular lipid peroxidation assay

Confocal microscopy: HeLa cells (5×10^5/well) were seeded in a 35 mm glass-bottom cell culture dish overnight. After incubating with Re(I) complexes for 6 h, cells were washed with serum-free DMEM twice and labelled with C11-BODIPY 581/591 (2 μM) for 30 min. Subsequently, cells were examined under confocal microscopy ($\lambda_{ex} = 488$ nm, $\lambda_{em} = 510 \pm 20$ nm (green); $\lambda_{ex} = 581$ nm, $\lambda_{em} = 591 \pm 20$ nm (red)).

Flow cytometry: HeLa cells were seeded in 6-well plates at a density of 1×10^6/well and incubated for 24 h. After that, cells were incubated with Re(I) complexes for 6 h and then washed with serum-free DMEM twice. After labelling with C11-BODIPY 581/591 (2 μM) for 30 min, cells were harvested and resuspended in 500 μL PBS. Flow cytometry was used to analyze cells.

4.19. Statistical analysis

The biological experiments were conducted at least 3 repetitions, and the data were reported as means ± SD.

Declaration of Competing Interest

The authors declare that they have no known competing financial interests or personal relationships that could have appeared to influence the work reported in this paper.

Acknowledgements

This work was supported by the National Natural Science Foundation of China (21967014, 22007042), Applied Basic Research Projects of Yunnan Province (202001AT070036), the Innovative Team of Yunnan Province (2019HC018), High-level Scientific Research Foundation for Talent Introduction of Kunming University of Science and Technology (KKKP201826008).

Appendix A. Supplementary data

Supplementary data to this article can be found online at https://doi.org/10.1016/j.jinorgbio.2021.111537.

References

[1] K.K. Lo, Acc. Chem. Res. 48 (2015) 2985–2995.
[2] L.C. Lee, K.K. Leung, K.K. Lo, Dalton Trans. 46 (2017) 16357–16380.
[3] F.F. Knapp Jr., Cancer Biother. Radiopharm. 13 (1998) 337–349.
[4] A. Leonidova, G. Gasser, ACS Chem. Biol. 9 (2014) 2180–2193.
[5] H.S. Liew, C.W. Mai, M. Zulkefeli, T. Madheswaran, L.V. Kiew, N. Delsuc, M. L. Low, Molecules 25 (2020) 4176.
[6] Z.Y. Pan, D.H. Cai, L. He, Dalton Trans. 49 (2020) 11583–11590.
[7] M.S. Capper, H. Packman, M. Rehkamper, ChemBioChem 21 (2020) 2111–2115.
[8] F.-X. Wang, J.-H. Liang, H. Zhang, Z.-H. Wang, Q. Wan, C.-P. Tan, L.-N. Ji, Z.-W. Mao, ACS Appl. Mater. Interfaces 11 (2019) 13123–13133.
[9] A.P. King, S.C. Marker, R.V. Swanda, J.J. Woods, S.B. Qian, J.J. Wilson, Chem. Eur. J. 25 (2019) 9206–9210.
[10] S.C. Marker, A.P. King, S. Granja, B. Vaughn, J.J. Woods, E. Boros, J.J. Wilson, Inorg. Chem. 59 (2020) 10285–10303.
[11] S.C. Marker, A.P. King, R.V. Swanda, B. Vaughn, E. Boros, S.B. Qian, J.J. Wilson, Angew. Chem. Int. Ed. 59 (2020) 13391–13400.
[12] P.V. Simpson, I. Casari, S. Paternoster, B.W. Skelton, M. Falasca, M. Massi, Chem. Eur. J. 23 (2017) 6518–6521.
[13] A. Domenichini, I. Casari, P.V. Simpson, N.M. Desai, L. Chen, C. Dustin, J. S. Edmands, A. van der Vliet, M. Mohammadi, M. Massi, M. Falasca, J. Exp. Clin. Cancer Res. 39 (2020) 276.
[14] J. Delasoie, A. Pavic, N. Voutier, S. Vojnovic, A. Crochet, J. Nikodinovic-Runic, F. Zobi, Eur. J. Med. Chem. 204 (2020) 112583.
[15] R.R. Ye, C.P. Tan, Y.N. Lin, L.N. Ji, Z.W. Mao, Chem. Commun. 51 (2015) 8353–8356.
[16] R.R. Ye, C.P. Tan, M.H. Chen, L. Hao, L.N. Ji, Z.W. Mao, Chem. Eur. J. 22 (2016) 7800–7809.
[17] D. Hanahan, R.A. Weinberg, Cell 144 (2011) 646–674.
[18] S. Banerjee, Y. Li, Z. Wang, F.H. Sarkar, Cancer Lett. 269 (2008) 226–242.
[19] N.S. Moorthy, N.M. Cerqueira, M.J. Ramos, P.A. Fernandes, Rec. Pat. Anticancer Drug Discov. 8 (2013) 168–182.
[20] A. Bergamo, G. Sava, Chem. Soc. Rev. 44 (2015) 8818–8835.
[21] N.S. Gul, T.M. Khan, M. Chen, K.B. Huang, C. Hou, M.I. Choudhary, H. Liang, Z. F. Chen, J. Inorg. Biochem. 213 (2020) 111260.
[22] Z.Y. Pan, C.P. Tan, L.S. Rao, H. Zhang, Y. Zheng, L. Hao, L.N. Ji, Z.W. Mao, Angew. Chem. Int. Ed. 59 (2020) 18755–18762.
[23] A.L. Greenshields, W. Fernando, D.W. Hoskin, Exp. Mol. Pathol. 107 (2019) 10–22.
[24] R.R. Ye, W. Peng, B.C. Chen, N. Jiang, X.Q. Chen, Z.W. Mao, R.T. Li, Metallomics 12 (2020) 1131–1141.
[25] J. Guo, B. Xu, Q. Han, H. Zhou, Y. Xia, C. Gong, X. Dai, Z. Li, G. Wu, Cancer Res. Treat. 50 (2018) 445–460.
[26] G. Kroemer, L. Galluzzi, P. Vandenabeele, J. Abrams, E.S. Alnemri, E.H. Baehrecke, M.V. Blagosklonny, W.S. El-Deiry, P. Golstein, D.R. Green, M. Hengartner, R. A. Knight, S. Kumar, S.A. Lipton, W. Malorni, G. Nuñez, M.E. Peter, J. Tschopp, J. Yuan, M. Piacentini, B. Zhivotovsky, G. Melino, Cell Death Differ. 16 (2009) 3–11.
[27] S.J. Dixon, K.M. Lemberg, M.R. Lamprecht, R. Skouta, E.M. Zaitsev, C.E. Gleason, D.N. Patel, A.J. Bauer, A.M. Cantley, W.S. Yang, B. Morrison, B.R. Stockwell, Cell 149 (2012) 1060–1072.
[28] S.E. Wenzel, Y.Y. Tyurina, J. Zhao, C.M. St Croix, H.H. Dar, G. Mao, V.A. Tyurin, T. S. Anthonymuthu, A.A. Kapralov, A.A. Amoscato, K. Mikulska-Ruminska, I. H. Shrivastava, E.M. Kenny, Q. Yang, J.C. Rosenbaum, L.J. Sparvero, D.R. Emlet, X. Wen, Y. Minami, F. Qu, S.C. Watkins, T.R. Holman, A.P. VanDemark, J. A. Kellum, I. Bahar, H. Bayır, V.E. Kagan, Cell 171 (2017) 628–641, e26.

[29] M. Gao, J. Yi, J. Zhu, A.M. Minikes, P. Monian, C.B. Thompson, X. Jiang, Mol. Cell 73 (2019) 354–363.
[30] H. Wang, C. Liu, Y. Zhao, G. Gao, Eur. J. Cell Biol. 99 (2020) 151058.
[31] A.M. Battaglia, R. Chirillo, I. Aversa, A. Sacco, F. Costanzo, F. Biamonte, Cells 9 (2020) 1505.
[32] A. Ayala, M.F. Munoz, S. Arguelles, Oxidative Med. Cell. Longev. 2014 (2014) 360438.
[33] H. Yu, P. Guo, X. Xie, Y. Wang, G. Chen, J. Cell. Mol. Med. 21 (2017) 648–657.
[34] W.S. Yang, R. SriRamaratnam, M.E. Welsch, K. Shimada, R. Skouta, V. S. Viswanathan, J.H. Cheah, P.A. Clemons, A.F. Shamji, C.B. Clish, L.M. Brown, A. W. Girotti, V.W. Cornish, S.L. Schreiber, B.R. Stockwell, Cell 156 (2014) 317–331.
[35] X. Wang, F. Chen, J. Zhang, J. Sun, X. Zhao, Y. Zhu, W. Wei, J. Zhao, Z. Guo, Sci. China Chem. 63 (2020) 65–72.
[36] J. Sagasser, B.N. Ma, D. Baecker, S. Salcher, M. Hermann, J. Lamprecht, S. Angerer, P. Obexer, B. Kircher, R. Gust, J. Med. Chem. 62 (2019) 8053–8061.
[37] Z. Kong, R. Liu, Y. Cheng, Biomed. Pharmacother. 109 (2019) 2043–2053.
[38] F.J. Bock, S.W.G. Tait, Nat. Rev. Mol. Cell Biol. 21 (2020) 85–100.
[39] S.F. He, N.L. Pan, B.B. Chen, J.X. Liao, M.Y. Huang, H.J. Qiu, D.C. Jiang, J.J. W, J. X. Chen, J. Sun, J. Biol. Inorg. Chem. 25 (2020) 1107–1116.
[40] A.A. Pizano, D.A. Lutterman, P.G. Holder, T.S. Teets, J. Stubbe, D.G. Nocera, Proc. Natl. Acad. Sci. U. S. A. 109 (2012) 39–43.
[41] V. Pierroz, T. Joshi, A. Leonidova, C. Mari, J. Schur, I. Ott, L. Spiccia, S. Ferrari, G. Gasser, J. Am. Chem. Soc. 134 (2012) 20376–20387.
[42] N. Jiang, J. Fan, T. Liu, J. Cao, B. Qiao, J. Wang, P. Gao, X. Peng, Chem. Commun. 49 (2013) 10620–10622.
[43] C. Li, M. Yu, Y. Sun, Y. Wu, C. Huang, F. Li, J. Am. Chem. Soc. 133 (2011) 11231–11239.
[44] R.C. Scaduto Jr., L.W. Grotyohann, Biophys. J. 76 (1999) 469–477.
[45] M. Poot, Y.Z. Zhang, J.A. Krämer, K.S. Wells, L.J. Jones, D.K. Hanzel, A.G. Lugade, V.L. Singer, R.P. Haugland, J. Histochem. Cytochem. 44 (1996) 1363–1372.
[46] L. He, K.N. Wang, Y. Zheng, J.J. Cao, M.F. Zhang, C.P. Tan, L.N. Ji, Z.W. Mao, Dalton Trans. 47 (2018) 6942–6953.
[47] M.C. Frantz, P. Wipf, Environ. Mol. Mutagen. 51 (2010) 462–475.
[48] D. Trachootham, J. Alexandre, P. Huang, Nat. Rev. Drug Discov. 8 (2009) 579–591.
[49] Y. Pang, G. Qin, L. Wu, X. Wang, T. Chen, Exp. Cell Res. 347 (2016) 251–260.
[50] C.P. LeBel, H. Ischiropoulos, S.C. Bondy, Chem. Res. Toxicol. 5 (1992) 227–231.
[51] R.C. Taylor, S.P. Cullen, S.J. Martin, Nat. Rev. Mol. Cell Biol. 9 (2008) 231–241.
[52] H. Kashkar, K. Wiegmann, B. Yazdanpanah, D. Haubert, M. Krönke, J. Biol. Chem. 280 (2005) 20804–20813.
[53] F.J. Oliver, G. de la Rubia, V. Rolli, M.C. Ruiz-Ruiz, G. de Murcia, J.M. Murcia, J. Biol. Chem. 273 (1998) 33533–33539.
[54] C.M. Simbulan-Rosenthal, D.S. Rosenthal, S. Iyer, A.H. Boulares, M.E. Smulson, J. Biol. Chem. 273 (1998) 13703–13712.
[55] J.Y. Cao, S.J. Dixon, Cell. Mol. Life Sci. 73 (2016) 2195–2209.
[56] Y. Wang, K. Xu, H.B. Zhang, J.H. Zhao, X.P. Zhu, Y.Z. Wang, R.Y. Wu, Mol. Med. Rep. 10 (2014) 1179–1183.
[57] B.R. Stockwell, J.P. Friedmann Angeli, H. Bayir, A.I. Bush, M. Conrad, S.J. Dixon, S. Fulda, S. Gascón, S.K. Hatzios, V.E. Kagan, K. Noel, X. Jiang, A. Linkermann, M. E. Murphy, M. Overholtzer, A. Oyagi, G.C. Pagnussat, J. Park, Q. Ran, C. S. Rosenfeld, K. Salnikow, D. Tang, F.M. Torti, S.V. Torti, S. Toyokuni, K. A. Woerpel, D.D. Zhang, Cell 171 (2017) 273–285.
[58] D.H. Manz, N.L. Blanchette, B.T. Paul, F.M. Torti, S.V. Torti, Ann. N. Y. Acad. Sci. 1368 (2016) 149–161.
[59] Y. Xie, W. Hou, X. Song, Y. Yu, J. Huang, X. Sun, R. Kang, D. Tang, Cell Death Differ. 23 (2016) 369–379.
[60] W.S. Yang, B.R. Stockwell, Trends Cell Biol. 26 (2016) 165–176.
[61] J.M. Smieja, C.P. Kubiak, Inorg. Chem. 49 (2010) 9283–9289.
[62] B. Machura, M. Wolff, M. Jaworska, P. Lodowski, E. Benoist, C. Carrayon, N. Saffon, R. Kruszynski, Z. Mazurak, J. Organomet. Chem. 696 (2011) 3068–3075.
[63] M.J. McKeage, S.J. Berners-Price, P. Galettis, R.J. Bowen, W. Brouwer, L. Ding, L. Zhuang, B.C. Baguley, Cancer Chemother. Pharmacol. 46 (2000) 343–350.